Hue University Journal of Science: Natural Science
Vol. 132, No. 1B, 83–91, 2023

pISSN 1859-1388
eISSN 2615-9678

# Non-doped phosphor for wled with high cri and $r_9$

**Dang Thi To Nu[1], Nguyen Minh Thong[2], Nguyen M.C.H.P. Lan[2], Dao Xuan Viet[2], Le Thi Thao Vien[1*]**

[1] Faculty of Natural Sciences, Quy Nhon University, 170 An Duong Vuong St., Quy Nhon, Binh Dinh, Vietnam
[2] International Training Institute for Materials Science (ITIMS), Hanoi University of Science and Technology (HUST), 1 Dai Co Viet St., Hanoi, Vietnam

* Correspondence to Le Thi Thao Vien <lethithaovien@qnu.edu.vn>

(*Received: 20 June 2022; Accepted: 10 October 2022*)

**Abstract.** The effect of the $ZnO/SnO_2$ ratio on phase formation and optical properties of the Zn-Sn-O compound was investigated by varying the $ZnO/SnO_2$ molar ratio ($ZnO/SnO_2$ = 1:2, 1:1, 2:1, 3:1, and 4:1). All samples were synthesised with high-energy planetary ball milling, followed by calcination at 1000 °C in the air. The result from X-Ray diffraction patterns (XRD) shows that the single-phase $Zn_2SnO_4$ was achieved at the $ZnO/SnO_2$ ratio of 2:1. Whereas, the mixed phase of ZnO and $Zn_2SnO_4$ formed when ZnO is more than $SnO_2$ (3:1 and 4:1). On the other hand, the XRD patterns of the products obtained at a ratio where $SnO_2$ is more than ZnO present a mixture of $SnO_2$ and $Zn_2SnO_4$. The photoluminescence of the two samples with the ratio of 2:1 and 1:3 gives full-visible range spectra from 400 to 800 nm, which are in the blue-far-red region centred at about 514, 580, and 690 nm. Temperature-dependent luminescence measurements were also carried out in this work, and the results indicate that the prepared phosphor Zn-Sn-O at the $ZnO/SnO_2$ ratio of 1:2 has thermal stability. The obtained material was used to coat near UV LED chips, and the WLED possesses the highest CRI of 95. The $SnO_2$-$Zn_2SnO_4$ powder can be used as a phosphor for WLED applications with high CRI and $R_9$.

**Keywords:** Zn-Sn-O compound, photoluminescence of $Zn_2SnO_4$, full visible range

## 1 Introduction

In recent years, metal oxide semiconductors (MOSs), in general, and Zn-Sn-O compounds, in particular, have attracted much attention from scientists because of their exciting properties in photocatalytic activity [1, 2], high electron mobility, high electrical conductivity, and attractive optical properties [3]. Depending on the ratio of the chemical composition of $ZnO/SnO_2$, Zn-Sn-O compounds have different phase formations. For instance, ZnO-$SnO_2$ nanocomposites have been produced with a $ZnO/SnO_2$ molar ratio equal to 1:0.05 by Hamrouni et al. [4] and other groups [5–7]. Besides, in Nakhanivej et al.'s previous report [3], the pure single-phase $Zn_2SnO_4$ was achieved at the mass ratio of 1:1, while the mixed phase of ZnO and $Zn_2SnO_4$ was formed when the portion of ZnO greater than that of $SnO_2$ (3:1 and 2:1). Among them, $Zn_2SnO_4$ is considered one of the most stable phases with an entirely inverse spinel structure in which $Zn^{2+}$ ions occupy tetrahedral voids and $Sn^{4+}$ ions randomly occupy octahedral voids [2, 8-14].

All phases of the Zn-Sn-O compounds have a wide bandgap of about 3.6 eV for the $Zn_2SnO_4$ phase [8, 15] or 3.29 eV for ZnO or $SnO_2$ [7]. Therefore, they have excellent optical properties, chemical response, low visible absorption, and excellent electronic properties that have numerous promising applications in solid light [8], gas sensors [15, 16], solar cells [11], and

photocatalysis [6, 17, 18]. However, compared with the widely reported solar cell and photocatalyst application for Zn-Sn-O compounds, there are few reports on their WLED application. In addition, the effect of the $ZnO/SnO_2$ ratio on phase formation and photoluminescence behaviour of the Zn-Sn-O compounds has rarely been reported. Moreover, the influence of various ratios of $ZnO/SnO_2$ on WLED parameters, such as colour rendering index (CRI), correlated colour temperature (CCT), and luminous efficacy of radiation (LER), has not been studied before.

To address these issues, we synthesised the Zn-Sn-O compounds with simple high-energy planetary ball milling, followed by calcination at 1000 °C in air. Besides, the effect of the $ZnO/SnO_2$ mass ratio on phase formation and photoluminescence properties was studied systemically by varying the $ZnO/SnO_2$ ratio (1:1, 1:2, 2:1, 1:3, 3:1) in the milling process. The last step was to coat a near UV LED chip with all the obtained samples and evaluate the WLEDs parameters related to their quality.

## 2 Experimental

Zinc oxide (ZnO) and tin (IV) dioxide ($SnO_2$) (Sigma-Aldrich) were selected for starting material sources. The process includes three steps: First, the mixture of ZnO and $SnO_2$ was introduced into a clean mortar for coarse grinding for 30 minutes. Then, the mixed powder was put into a Restch PM400 machine for high-energy planetary ball milling for 10 hours. Finally, the mixture was calcinated at 1,000 °C for exemplary phosphor.

X-ray diffraction (XRD) with CuK$\alpha$ (Bruker D8 Advance) as an X-ray source with a wavelength of 1.5604 Å was used to characterise the structure of all produced samples. Ultra-high-resolution scanning electron microscopy (FESEM Jeol JSM-7600F) was used to study surface morphology and particle sizes. The optical properties of all obtained products were examined by using photoluminescence spectra (PL) and 3D photoluminescence spectra (3D PL). The produced phosphors were coated directly onto a near UV LED chip by using the i-DR S320A Desktop Dispensing system, and the fabricated LEDs' parameters were measured with the integral sphere and Colorcalculator-32 system.

## 3 Results and discussion

### 3.1 Effect of $ZnO/SnO_2$ ratio on structure and surface morphology of Zn-Sn-O compounds

Fig. 1 shows X-ray diffraction patterns of all samples obtained with different $ZnO/SnO_2$ ratios. Overall, the crystal phase formation of the Zn-Sn-O compounds is significantly affected by the varying ratios of $ZnO/SnO_2$ (1:2, 1:1, 2:1, 3:1, and 4:1) in the process. It is clear to see from Fig. 1 that the single-phase of the $Zn_2SnO_4$ material has been formed at the $ZnO/SnO_2$ ratio of 2:1. All the diffraction peaks are indexed to the cubic phase $Zn_2SnO_4$ (JCPDS card no. 00-024-1470, space group Fd-3m (227), and cell parameters $a = b = c =$ 8.7125 Å) [19] and the majority peaks positioned

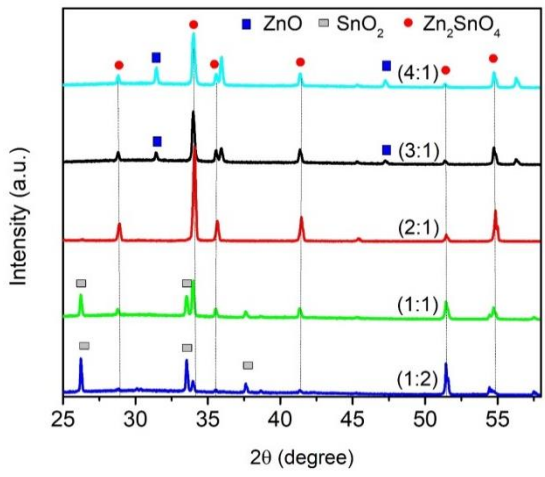


**Fig. 1.** XRD patterns of the Zn-Sn-O samples fabricated with different $ZnO/SnO_2$ ratios

pISSN 1859-1388
eISSN 2615-9678

at 28.62, 33.80, 35.32, 41.17, 54.44, and 59.83° can be attributed to the (220), (311), (222), (400), (511), and (440) planes, respectively.

This result is in good agreement with previous work by Dimitrievska et al. [9]. Using the high-energy planetary ball milling method, these authors reported that their energy-dispersive X-ray spectroscopy (EDXS) measurements of the sample obtained at 1,200 °C shows the Zn/Sn compositional ratios of 1.9 and 1.95 for the undoped and Eu-doped $Zn_2SnO_4$ samples. Compared with this result, our work gets a good $Zn_2SnO_4$ phase at a calcination temperature of 200 °C lower. The reason possibly belongs to the difference in milling time and speed. For the mixtures with more ZnO than $SnO_2$ ($ZnO/SnO_2$ ratio at 3:1 and 4:1), the XRD patterns show the mixed phase of ZnO and $Zn_2SnO_4$, which can be assigned to excessive Zn ion participation in the solid-state reaction. All the diffraction peaks are indexed to the cubic phase $Zn_2SnO_4$ (JCPDS card No. 00-024-1470, space group Fd-3m (227), and cell parameters $a = b = c =$ 8.657 Å) [19] and hexagonal phase ZnO (JCPDS card No. 00-005-0664, space group P63mc (186), and cell constants $a = b =$ 3.249 Å and $c =$ 5.205 Å) [20]. Whereas, the samples where $SnO_2$ is more than ZnO ($ZnO/SnO_2$ ratio at 1:2 and 1:1), the XRD patterns present a mixed phase of $SnO_2$ and $Zn_2SnO_4$ because of the excessive Sn ion participation in the solid-state. All the diffraction peaks are indexed to the $Zn_2SnO_4$ cubic phase (JCPDS card No. 00-024-1470, space group Fd-3m (227), and cell parameters $a = b = c =$ 8.657 Å) [19] and tetragonal phase $SnO_2$ (JCPDS card No. 00-021-1250, space group P42/mm (136), and cell constants $a = b =$ 4.738 Å and $c =$ 3.188 Å) [21].

To study the surface morphology and particles size of the produced samples obtained at different $ZnO/SnO_2$ ratios, we used ultra-high-resolution field emission scanning electron microscopy (FESEM), and the results are shown in Fig. 2. It is obvious that all samples have spherical particles. The average particle size is in the range of 0.2–0.5 μm, and a big size difference exists among the samples. Meanwhile, $ZnO/SnO_2$ ratios significantly affect surface morphology and particle size. The change in the grain size may be due to the difference in the reaction temperature between ZnO and $SnO_2$ because all samples were produced under the same conditions, such as milling time, calcination temperature, rotation speed, and annealing time.

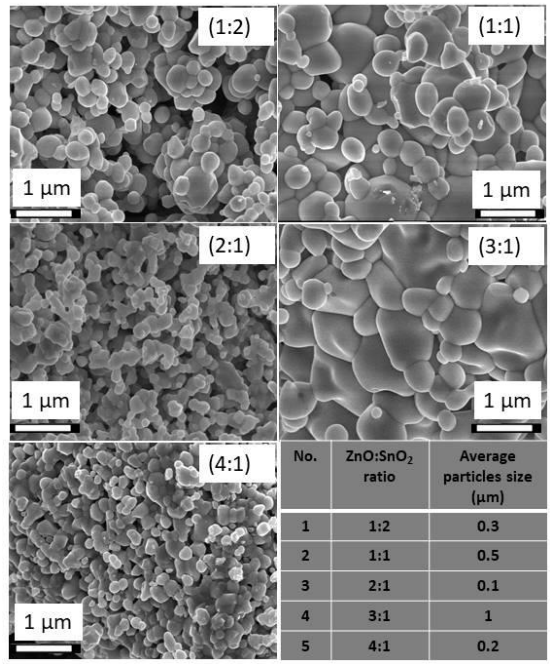


| No. | $ZnO:SnO_2$ ratio | Average particles size (μm) |
|---|---|---|
| 1 | 1:2 | 0.3 |
| 2 | 1:1 | 0.5 |
| 3 | 2:1 | 0.1 |
| 4 | 3:1 | 1 |
| 5 | 4:1 | 0.2 |

**Fig. 2.** FESEM images of the Zn-Sn-O sample obtained at different $ZnO/SnO_2$ ratios and calcination temperature of 1,000 °C

The energy-dispersive X-ray spectroscopy (EDXS) was used to check the atom composition and chemical composition of the samples, and the obtained results are represented in Fig. 3. Three elements: zinc (Zn), tin (Sn), and oxygen (O) are present in the as-prepared Zn-Sn-O compound, confirming fine pure phosphor. Besides, the element atom composition of all prepared samples is shown in the EDXS data (the table in Fig. 3). For the $ZnO/SnO_2$ ratio of 2:1, the atom composition of Zn, Sn, and O is 27.8, 13.2 and 59%, respectively, showing a suitable ratio to form

$Zn_2SnO_4$. When there is more ZnO than $SnO_2$ (ZnO/$SnO_2$ ratio of 3:1 and 4:1), the EDS data demonstrate that the Zn atoms are excessive during phase transformation, while the excess of the Sn atoms is present in the inverted case.

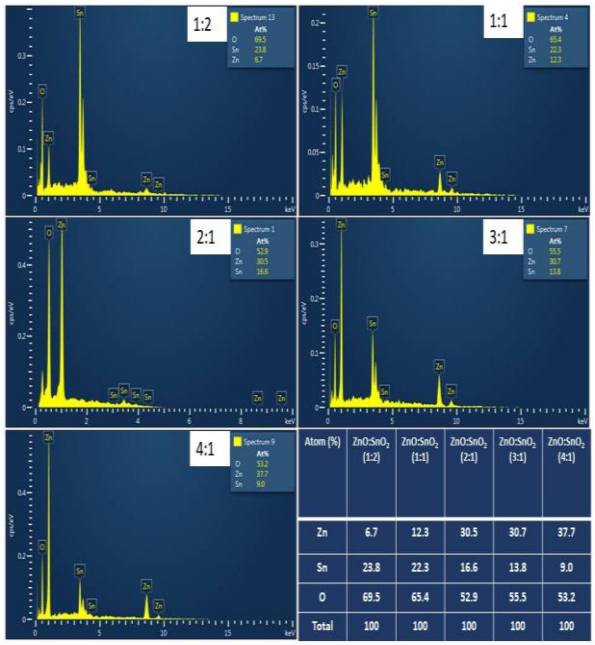


| Atom (%) | ZnO:SnO$_2$ (1:2) | ZnO:SnO$_2$ (1:1) | ZnO:SnO$_2$ (2:1) | ZnO:SnO$_2$ (3:1) | ZnO:SnO$_2$ (4:1) |
|---|---|---|---|---|---|
| Zn | 6.7 | 12.3 | 30.5 | 30.7 | 37.7 |
| Sn | 23.8 | 22.3 | 16.6 | 13.8 | 9.0 |
| O | 69.5 | 65.4 | 52.9 | 55.5 | 53.2 |
| Total | 100 | 100 | 100 | 100 | 100 |

**Fig. 3.** EDS spectra of the Zn-Sn-O sample obtained at different ZnO/$SnO_2$ ratios and calcination temperature of 1,000 °C

### 3.2 Effect of ZnO/$SnO_2$ ratio on optical properties of Zn-Sn-O compounds

The band gap, $E_g$, is one of the essential factors affecting the optical properties of a phosphor. To evaluate how various ZnO/$SnO_2$ ratios affect the bandgap change of the materials, we recorded the UV-Vis spectra of all prepared samples in the wavelength range of 200–700 nm, examined optical properties, and estimated the band gap of the samples (Fig. 4).

To determine the band gap of all samples obtained at different ZnO/$SnO_2$ ratios, we used Tauc's formula [22].

Typically, a Tauc's plot shows the quantity $h\nu$ (the energy of light) on the abscissa and the quantity $(\alpha h\nu)^{1/r}$ on the ordinate as formula (1)

$$(\alpha \times h \times \nu)^{1/r} = K \times (h \times \nu - E_g) \quad (1)$$

where $\alpha$ is the absorption coefficient of the material. The value of the exponent $r$ denotes the nature of the transition where $r$ = 1/2 for direct allowed transitions and $r$ = 2 for indirect allowed transitions.

It is known that ZnO, $Zn_2SnO_4$, and $SnO_2$ are direct semiconductors [22, 12] and hence, by plotting $(\alpha \times h \times \nu)^2$ versus $h \times \nu$, we can determine the optical band gap by extrapolating the linear portion with $(h \times \nu)$ axis when $(\alpha \times h \times \nu)^2 = 0$, as given in the inset of Fig. 4.

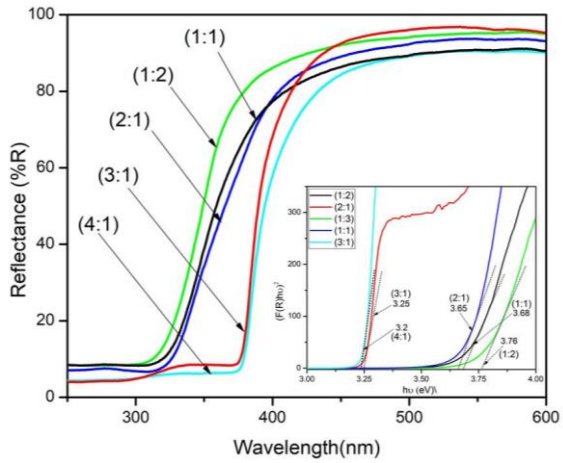


**Fig. 4.** UV-Vis spectra of the Zn-Sn-O samples obtained at different ZnO/$SnO_2$ ratios and calcination temperature of 1,000 °C

For the sample obtained at the ZnO/$SnO_2$ ratio of 2:1, the band gap is 3.65 eV, approximately equal to that of bulk $Zn_2SnO_4$ (3.6 eV) [23, 24]. However, for the samples with more ZnO than $SnO_2$ (ZnO/$SnO_2$ ratio of 3:1 and 4:1), their estimated band gap value is slightly smaller at 3.25 and 3.2 eV. As pointed out in the XRD result, X-ray diffraction patterns for ZnO/$SnO_2$ at the ratios of 3:1 and 4:1 show two mixed phases of ZnO and $Zn_2SnO_4$ because of the Zn ion excess in the solid-state reaction. Therefore, we suggest that the ZnO phase causes the band gap of these two samples to decrease. Nevertheless, the estimated band gap of the samples with more $SnO_2$ than

pISSN 1859-1388
eISSN 2615-9678

ZnO ($ZnO/SnO_2$ ratio at 1:1 and 1:2) is larger than that in the two other cases (3.68 and 3.76 eV). The increase of band gap may be due to the appearance of the $SnO_2$ (3.7 eV) [26] phase, causing the Sn ion excess to appear in the solid-state reaction, as analysed in the previous XRD results.

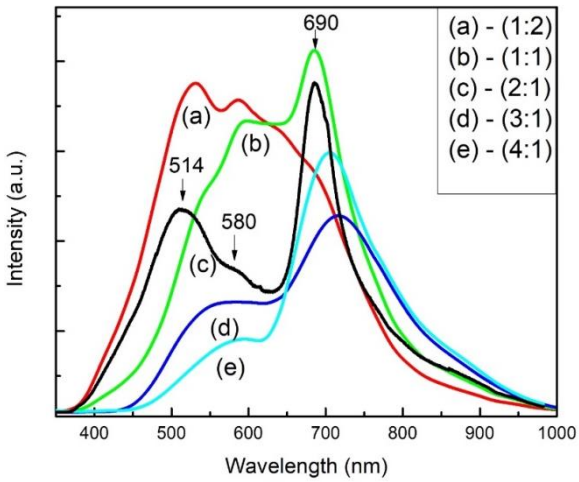


**Fig. 5.** PL spectra of the Zn-Sn-O samples obtained at different $ZnO/SnO_2$ ratios and calcination temperature of 1,000 °C

The PL spectra at room temperature were measured by using Nanolog – Horiba Jobin Yvon equipment with an excitation wavelength of 310 nm. Fig. 5 represents the PL spectra of the Zn-Sn-O samples obtained at different $ZnO/SnO_2$ ratios and at the calcination temperature of 1,000 °C. As can be seen from Fig. 5, the PL spectra of all samples obtained at various ratios of $ZnO/SnO_2$ show a strong and broad emission band from 400 to 1,000 nm with three peaks. The first and second peaks appear in the green-orange region at 514 and 580 nm, and the last peak is at 690 nm, corresponding to the red region. According to Zhao et al. [27, 28], the first peak is attributed to oxygen vacancies in the host lattice $Zn_2SnO_4$ and is responsible for the green emission band. Meanwhile, Das et al. and other reports [2, 29] confirmed that oxygen vacancy in the ZnO lattice is responsible for the green emission (520 nm). Nevertheless, the $SnO_2$ nanowires produced by Domashevskaya et al. show stable photoluminescence (PL) with one emission peak centred at around 2 eV (591 nm), which is associated with oxygen vacancies or surface defect states in $SnO_2$ [30]. For our results, we conclude that the green-orange region at 514 and 580 nm may be due to the contribution of oxygen vacancies in the host $Zn_2SnO_4$ lattice at the $ZnO/SnO_2$ ratio of 2:1, while for the $ZnO/SnO_2$ samples with the ratio of 1:1 and 1:2, the two emission bands belong to both oxygen vacancies in the host $Zn_2SnO_4$ lattice and oxygen vacancies in $SnO_2$. Indeed, as can be seen from Fig. 5, the PL intensity of the peaks at 514 and 580 nm increases with the amount of $SnO_2$, while the PL intensity of these two peaks decreases for the $ZnO/SnO_2$ ratios of 3:1 and 4:1, when ZnO is more then $SnO_2$. Furthermore, the excitation photoluminescence (PLE) of the $ZnO/SnO_2$ 1:1 and 1:2 samples shows strong peak absorption at about 330 nm, close to the band gap of $SnO_2$ (Fig. 6). Meanwhile, we suggest that the origin of the green-orange region at 512 and 580 nm is related to oxygen vacancies in $SnO_2$.

The nature of the far-red emission (690 nm) is still questionable. Hu et al. claimed that the origin of the unusual 630 nm emission band is related to the Sn and Zn vacancies in $Zn_2SnO_4$ phosphor powder. Whereas, Fu et al. [31] approved that stoichiometry Zn/Sn plays a role in this emission. In this work, we speculate that the red emission peak at 690 nm is attributed to the crystal quality of the $Zn_2SnO_4$ phase. Specifically, we suggest that this far-red emission belongs to the surface defects of the Zn vacancies instead of the Sn vacancies in $Zn_2SnO_4$. Indeed, as shown in PL spectra (Fig. 5), the intensity of the 690 nm peak of the two samples with a Zn ion excess is lower than that of the other samples. This may be explained by the fact that the Zn vacancies in $Zn_2SnO_4$ are filled with extra Zn ions, and, thus, reducing the PL intensity. By contrast, for the

samples with more $SnO_2$ than ZnO, Zn vacancies appeared during the process, and the Zn vacancies due to the lack of Zn ion caused the increase of PL intensity. However, when the amount of $SnO_2$ increases to a $ZnO/SnO_2$ ratio of 1:3, the excess of Sn may fill up the Zn vacancies because of their close ionic radii (0.74 nm for $Zn^{2+}$ and 0.69 nm for $Sn^{4+}$), resulting in the reduction of the PL intensity in this sample. In addition, the effect of different $ZnO/SnO_2$ ratios on the absorption spectra of obtained samples was examined by using the PLE spectra, as given in Fig. 6. The spectra show that for the $ZnO/SnO_2$ at 3:1 and 4:1 ratio samples, the PLE spectra present a high peak at 380 nm (3.26 eV), corresponding to the band emission of ZnO while it is not observed for other samples. This result is in good agreement with the XRD and EDS results. Furthermore, this figure also shows that the suitable excitation wavelengths for all samples are in the UV range (270–320 nm), and, therefore, we used UV-LED chips as an excitation source for creating WLED by coating with the prepared phosphors.

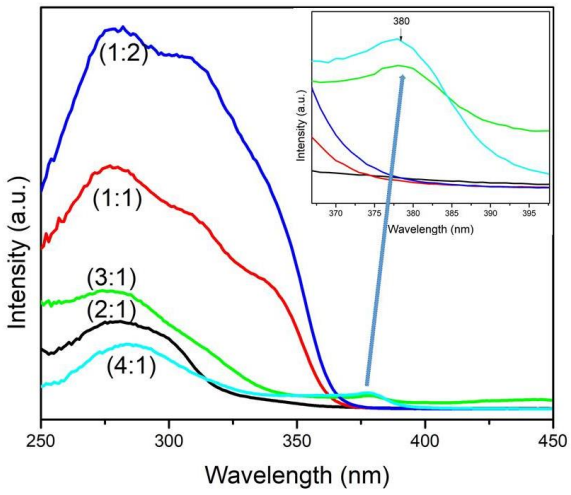


**Fig. 6.** PLE spectra of the Zn-Sn-O samples obtained at different $ZnO/SnO_2$ ratios and calcination temperature of 1,000 °C

In this part, we coat the UV-LED chips with the prepared phosphors and evaluate the LEDs' parameters. The PL spectra and CIE coordinates of the Zn-Sn-O samples obtained at different $ZnO/SnO_2$ ratios are presented in Fig. 7, and all LED indices are evaluated by using Colorcalculator-32 software (Table 1).

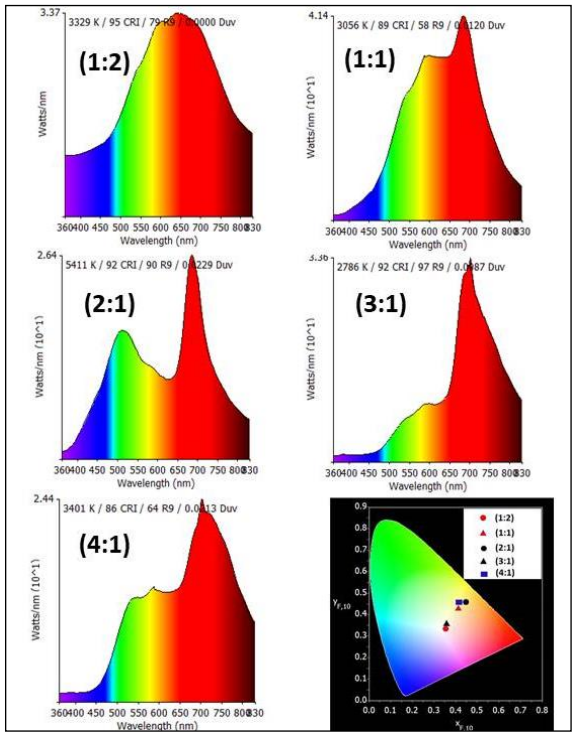


**Fig. 7.** PL spectra and CIE colour coordinates of the Zn-Sn-O samples obtained at different $ZnO/SnO_2$ ratios and calcination temperature of 1,000 °C

The calculated colour coordinates ($x$, $y$) for various ratios of $ZnO/SnO_2$ (1:2, 1:1, 2:1, 3:1, and 4:1) samples are as follows: $x$ = 0.3693, $y$ = 0.3707; $x$ = 0.4515, $y$ = 0.4409; $x$ = 0.3757, $y$ = 0.3852; $x$ = 0.4685, $y$ = 0.4349; and $x$ = 0.4375, $y$ = 0.4579, respectively (Table 1). As can be seen from CIE values, the colour coordinates of the $ZnO/SnO_2$ samples at the 3:1 and 1:2 ratios are close to natural white light. Besides, some WLED's parameters ($D_{uv}$, correlated colour temperature, colour rendering index, and CIE coordinates ($x$, $y$)) are given in Table 1. We can see from Table 1 that the $ZnO/SnO_2$ sample with a ratio of 1:2 has the highest value of colour rendering index (95)

pISSN 1859-1388
eISSN 2615-9678

and good colour temperature (4,277 K), which is energizing and most closely mimics natural daylight. Besides, the values of CRI at 92 and CCT at 5,043 K belong to the 2:1 ratio sample. Hence, these results demonstrate that we can change the ratio of $ZnO/SnO_2$ to get high CRI in WLEDs.

It is evident that sunlight is a natural source with colour temperature and high CRI at 5,600 K and 100. The CRI values of all obtained samples with various $ZnO/SnO_2$ ratios (1:2, 1:1, 2:1, 3:2, and 4:1) were measured and compared with the CRI value of the sunlight (Fig. 8). As shown in the figure, the $R_i$ value of the $ZnO/SnO_2$ samples at the 1:2 and 2:1 ratios is closer to that of sunlight than others. And hence, we can conclude that these samples are the most suitable for transparent luminescent layers and for white LEDs.

**Table 1.** WLED parameters ($D_{uv}$, correlated colour temperature (CCT), colour rendering index (CRI), luminous efficacy of radiation (LER), and CIE coordinates ($x$, $y$)) of LED covered with phosphor

| Sample | CCT (K) | CRI ($R_a$) | $x$ | $y$ | $D_{uv}$ |
|---|---|---|---|---|---|
| **$ZnO/SnO_2$ (1:2)** | 4,277 | 95 | 0.3693 | 0.3707 | 0.0006 |
| **$ZnO/SnO_2$ (1:1)** | 3,049 | 89 | 0.4515 | 0.4409 | 0.0120 |
| **$ZnO/SnO_2$ (2:1)** | 5,043 | 92 | 0.3757 | 0.3852 | 0.0053 |
| **$ZnO/SnO_2$ (3:1)** | 2,764 | 92 | 0.4685 | 0.4349 | 0.0080 |
| **$ZnO/SnO_2$ (4:1)** | 3,383 | 86 | 0.4375 | 0.4579 | 0.0203 |

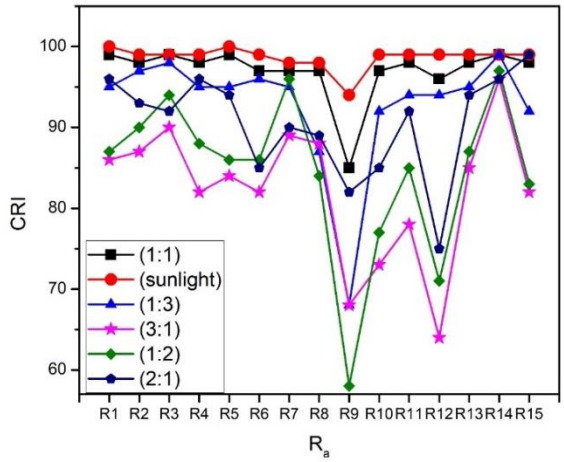


**Fig. 8.** Comparison of $R_i$ values of prepared samples with different $ZnO/SnO_2$ ratios and the sunlight

## 4 Conclusion

In this study, we report the effect of $ZnO/SnO_2$ ratio on phase formation and photoluminescence properties of the Zn-Sn-O compounds. For the phase formation, the pure single phase $Zn_2SnO_4$ was achieved at the $ZnO/SnO_2$ ratio of 2:1, while either ZnO or $SnO_2$ phase could be observed if there was a Zn or Sn ion excess in the synthesis system. The particles size was 0.2–0.5 μm with spherical morphology. The material with the $ZnO/SnO_2$ ratio of 2:1 had a band gap of 3.65 eV. This parameter could be be smaller or larger depending on Zn or Sn ion excess in the solid-state reaction. The $ZnO/SnO_2$ ratio also caused the change of both emission and absorption properties of the obtained samples. For the $ZnO/SnO_2$ ratios of 2:1 and 1:2, the photoluminescence gave full sunlight spectrum from 400 to 800 nm, and the blue-far-red region

centered at about 514, 580, and 690 nm. The UV LED Chip covered with the material at the $ZnO/SnO_2$ ratio of 1:2 exhibits the colour rendering index at 95 and a colour temperature of 4,277 K, which is energizing and most closely mimics natural daylight.

## Funding statement

This research is funded by Quy Nhon University under grand No. T2022.747.03

## References

1. Sun G, Zhang S, Li Y. Solvothermal synthesis of $Zn_2SnO_4$ nanocrystals and their photocatalytic properties. International Journal of Photoenergy. 2014.
2. Das PP, Roy A, Tathavadekar M, Devi PS. Photovoltaic and photocatalytic performance of electrospun $Zn_2SnO_4$ hollow fibers. Applied Catalysis B: Environmental. 2017;203:692-703.
3. Nakhanivej P, Tangcharoen T, Mekprasart W, Pecharapa W. Effect of Zn: Sn Ratio and Calcination Temperature on Phase Transformation of Zn-Sn-O Compound. InKey Engineering Materials. 2016;675: 539-543.
4. Hamrouni A, Moussa N, Parrino F, Di Paola A, Houas A, Palmisano L. Sol–gel synthesis and photocatalytic activity of $ZnO–SnO_2$ nanocomposites. Journal of Molecular Catalysis A: Chemical. 2014;390:133-41.
5. Ren L, Chen D, Hu Z, Gao Z, Luo Z, Chen Z, et al. Facile fabrication and application of $SnO_2–ZnO$ nanocomposites: insight into chain-like frameworks, heterojunctions and quantum dots. RSC advances. 2016;6(85):82096-102.
6. Ali W, Ullah H, Zada A, Alamgir MK, Muhammad W, Ahmad MJ, et al. Effect of calcination temperature on the photoactivities of $ZnO/SnO_2$ nanocomposites for the degradation of methyl orange. Materials Chemistry and Physics. 2018;213:259-66.
7. Zargar RA, Bhat MA, Parrey IR, Arora M, Kumar J, Hafiz AK. Optical properties of $ZnO/SnO_2$ composite coated film. Optik. 2016;127(17):6997-7001.
8. Chembanthodi Kuttykrishnan KS, Mohammed JB. Hydrothermal growth of $Zn_2SnO_4$: Eu, Ca for red emission. Luminescence. 2018;33(4):675-80.
9. Dimitrievska M, Ivetić TB, Litvinchuk AP, Fairbrother A, Miljević BB, Štrbac GR, Rodríguez AP, Lukić-Petrović SR. Supporting information for: Eu 3-doped Wide- Bandgap $Zn_2SnO_4$ Semiconductor Nanoparticles: Structure and Luminescence. The Journal of Physical Chemistry C. 2016.
10. Liu X, Chueh CC, Zhu Z, Jo SB, Sun Y, Jen AK. Highly crystalline $Zn_2SnO_4$ nanoparticles as efficient electron-transporting layers toward stable inverted and flexible conventional perovskite solar cells. Journal of Materials Chemistry A. 2016;4(40):15294-301.
11. Das PP, Roy A, Agarkar S, Devi PS. Hydrothermally synthesized fluorescent $Zn_2SnO_4$ nanoparticles for dye sensitized solar cells. Dyes and Pigments. 2018;154:303-313.
12. Dinesh S, Barathan S, Premkumar VK, Sivakumar G, Anandan N. Hydrothermal synthesis of zinc stannate ($Zn_2SnO_4$) nanoparticles and its application towards photocatalytic and antibacterial activity. Journal of Materials Science: Materials in Electronics. 2016;27(9):9668-75.
13. Dimitrievska M, Ivetić TB, Litvinchuk AP, Fairbrother A, Miljević BB, et al. $Eu^{3+}$-doped wide band gap $Zn_2SnO_4$ semiconductor nanoparticles: structure and luminescence. The Journal of Physical Chemistry C. 2016;120(33):18887-18894.
14. Baruah S, Dutta J. Zinc stannate nanostructures: hydrothermal synthesis. Science and technology of advanced materials. 2011.
15. Masjedi-Arani M, Salavati-Niasari M. Facile precipitation synthesis and electrochemical evaluation of Zn2SnO4 nanostructure as a hydrogen storage material. International Journal of Hydrogen Energy. 2017;42(17):12420-9.
16. Ma L, Ma SY, Kang H, Shen XF, Wang TT, Jiang XH, et al. Preparation of Ag-doped $ZnO-SnO_2$ hollow nanofibers with an enhanced ethanol sensing performance by electrospinning. Materials Letters. 2017;209:188-92.
17. Shatnawi M, Alsmadi AM, Bsoul I, Salameh B, Mathai M, Alnawashi G, et al. Influence of Mn doping on the magnetic and optical properties of ZnO nanocrystalline particles. Results in Physics. 2016;6:1064-1071.

pISSN 1859-1388
eISSN 2615-9678

18. Yang HM, Ma SY, Yang GJ, Chen Q, Zeng QZ, Ge Q, et al. Synthesis of $La_2O_3$ doped $Zn_2SnO4$ hollow fibers by electrospinning method and application in detecting of acetone. Applied Surface Science. 2017;425:585-93.

19. JCPDS card no. 00-024-1470.

20. JCPDS card no. 00-005-0664.

21. JCPDS card no. 00-024-1470.

22. Tauc J. Optical properties and electronic structure of amorphous Ge and Si. Materials research bulletin. 1968;3(1):37-46.

23. Jia T, Zhao J, Fu F, Deng Z, Wang W, Fu Z, et al. Synthesis, characterization, and photocatalytic activity of Zn-doped $SnO_2/Zn_2SnO_4$ coupled nanocomposites. International Journal of Photoenergy. 2014;2014.

24. Joseph LA, Jeronsia JE, Jaculine MM, Das SJ. Investigations on structural and optical properties of hydrothermally synthesized $Zn_2SnO_4$ nanoparticles. Physics Research International. 2016;2016.

25. Zhang J, Zhang B, Chen X, Mi B, Wei P, Fei B, et al. Antimicrobial bamboo materials functionalized with ZnO and graphene oxide nanocomposites. Materials. 2017;10(3):239.

26. Tharsika T, Haseeb AS, Akbar SA, Sabri MF, Hoong WY. Enhanced ethanol gas sensing properties of $SnO_2$-core/ZnO-shell nanostructures. Sensors. 2014;14(8):14586-600.

27. Hu QR, Jiang P, Xu H, Zhang Y, Wang SL, Jia X, et al. Synthesis and photoluminescence of $Zn_2SnO4$ nanowires. Journal of Alloys and Compounds. 2009;484(1-2):25-7.

28. Li Q, Wang Y, Wang D, Guo W, Zhang F, Wang C, et al. Preparation of $Zn_2SnO_4/SnO_2@$ $Mn_2O_3$ Microbox Composite Materials with Enhanced Lithium-Storage Properties. ChemElectroChem. 2017;4(6):1334-40.

29. Wu P, Li Q, Zou X, Cheng W, Zhang D, Zhao C, et al. Correlation between photoluminescence and oxygen vacancies in $In_2O_3$, $SnO_2$ and ZnO metal oxide nanostructures. InJournal of Physics: Conference Series 2009;188(1):012054.

30. Hadia NM, Ryabtsev SV, Domashevskaya EP, Seredin PV. Structure and photoluminescence properties of $SnO_2$ nanowires synthesized from SnO powder. The European Physical Journal-Applied Physics. 2009;48(1).

31. Yakami BR, Poudyal U, Nandyala SR, Rimal G, Cooper JK, Zhang X, et al. Steady state and time resolved optical characterization studies of $Zn_2SnO_4$ nanowires for solar cell applications. Journal of Applied Physics. 2016;120(16):163101.